Glazing and Winter Comfort
Part 2: An Advanced Tool for Complex Spatial and Temporal Conditions

Christopher Mackey, Vera Baranova, Lynn Petermann, M. Alejandra Menchaca-Brandan
Payette Associates, United States of America

Abstract

Of the factors that influence wintertime occupant thermal comfort, two are often of primary concern around cold windows: overall low mean radiant temperatures and localized downdraft currents. To prevent these from leading to a thermally uncomfortable environment in cold climates, the building industry has traditionally applied perimeter heating – a system that can be costly to maintain and can result in greater energy use by delivering heat directly to the envelope. At present, the decision to remove perimeter heat in cases of highly insulated envelopes typically relies on conservative rules of thumb or time-consuming simulation methods. This paper expands upon the method to address this in Part 1 and makes it applicable to the variety of non-standard spatial conditions that exist in real buildings. Additionally, it presents methods to address temporal variations that result from different climate conditions, occupancy periods, and non-steady state building physics. Ultimately, these methods are combined into a plugin for the Rhinoceros 3D modelling interface, which is a primary geometry-modelling engine for architects, allowing goals of removing perimeter heat to remain relevant throughout the design process.

Introduction

While the building industry has traditionally addressed discomfort near glazing in cold climates through the application of perimeter heat, the recent increased interest in energy efficiency and comfort has challenged this practice with a powerful question: What facade properties would provide warm enough interior surface temperatures to fully mitigate thermal discomfort and merit the removal of perimeter heat? Given that the answer to this question should account for both full-body thermal discomfort and local draft discomfort, design projects seeking this answer have traditionally required either a time-intensive computational fluids dynamics (CFD) simulation (Svidt and Heiselberg, 1995) or have relied on rules of thumb that have been proven to be overly-conservative (Schellen, 2016; Toftum et al., 2003). As a result, the practice could benefit from a method that gives more precise results than a rule of thumb but can be calculated in a shorter timeframe than CFD, enabling sufficient iteration through design options.

A simplified web tool, such as that presented in Part 1 of this work (Menchaca-Brandan et al., 2017), addresses this in a manner that provides real-time feedback with quickly solved equations. This enables designers and engineers to test the feasibility of removing perimeter heat early in the design process. It also helps designers devise general strategies for addressing occupant discomfort through either smaller glazing quantities or decreased window U-Value. However, as facade and building systems develop through design, they often become more complex such that they are no longer accommodated by this tool's simple assumptions. For example, there are a variety of spatial conditions that exist in most real buildings, which cannot be addressed with the simple methods of the web tool including:

- Non-Rectangular windows.
- Windows of varied heights within a single façade.
- Corners of the building.
- Walls that are not within a single plane (ie. staggered, crenelated, or curved facades).
- Conditions where interior furniture or geometry blocks the radiant view to windows.

Furthermore, the web interface lacks a means of accounting for non-steady state building physics and thus cannot advise on cases where these is an integral part of the design. Cases that would fall under this include:

- Radiant floors.
- Thermally massive solar heated spaces.
- Spaces where stratification is an intentional part of the HVAC design (ie. displacement ventilation).

Because of these limitations, practitioners would still need to run a time-consuming CFD simulation or revert to rules of thumb at the end of design to be certain that their non-standard building situations meet the original goals for removing perimeter heat. In order to avoid this and provide a fast but detailed means of winter comfort evaluation, this paper presents a method that uses the same core comfort and building physics functions of the web tool in a manner that accommodates a much wider range of geometric and temporal inputs. As a result, the designer has a means of evaluating these complex situations within the timeframe of a typical design project.

The ultimate hallmark of such a method that accommodates the complex conditions of the real world is a spatial map of thermal comfort over the floor plan of a building. Such a detailed map enables a designer or engineer to understand the regions of greatest thermal discomfort and test strategies to minimize the problematic areas. Several researchers have developed sub-zone thermal comfort mapping in the past (Newsham, 1995; Webb, 2013; Hoyt et al., 2014) and have successfully mapped the variations in mean radiant temperature (MRT) that exist over a room that result of cold window surfaces. However, these studies have a notable geometric limitation in that they are only applicable to box-shaped rooms where their rectangular solid angle calculations for view factor are applicable. Rakha (2015)

has used ray-tracing methods to calculate view factors to a wider array of geometric cases and has been able to map MRT for environments that are more complex. However, this MRT mapping was specifically for outdoor cases and has not yet been generalized to indoor cases. Perhaps the most notable of the shortcomings in existing methods is that there is no tool to describe downdraft speeds over a room other than CFD. As noted, previously, CFD simulation of downdraft plumes is often very time consuming and requires expertise to produce sufficiently accurate results. As a result, its application to the issue of perimeter heat is not currently feasible for the majority of projects in the industry and a simpler parametrization to estimate draft speeds would be helpful. While such parametrizations have been developed and validated (Heiselberg, 1994; Manz and Frank, 2003), they have not been generalized in order to map downdraft discomfort over the entire floor plan.

In addition to the lack of methods to generate spatial maps of discomfort, standard methods for addressing the temporal variations in climate, occupancy, and transient building physics are also lacking. Accordingly, this paper will first elaborate a series of methods for generating detailed spatial maps of wintertime thermal comfort followed by a set of temporal methods for the selection of design conditions. After this, validations will be presented for the methods that require it and a tool that integrates these methods into the Rhinoceros 3D design software of the architect will be described. Finally, the limitations of the tool will be discussed and key findings of the tool will be elaborated.

Spatial Methods

Mean Radiant Temperature with Complex Geometry

The PMV comfort model, which is intended for evaluation of full-body thermal sensations on the indoors, requires an input of MRT (ASHRAE, 2010). Typically, MRT is computed using the following formula:

$$MRT = \left[\sum_{i=1}^{N} F_i T_i^4 \right]^{1/4} \qquad (1)$$

Where F is the fraction of the spherical view occupied by a given indoor surface and T is the temperature of the surface. N refers to the number of surfaces within the room, indicating that the equation above is summed for all surfaces surrounding an occupant. Many historic MRT tools have calculated the view factor to each surface using rectangular solid angles using the following equation (Chrenko, 1953):

$$\Omega = \tan^{-1}\left(\frac{ac}{zp_1}\right) + \tan^{-1}\left(\frac{bc}{zp_2}\right) + \tan^{-1}\left(\frac{bd}{zp_3}\right) + \tan^{-1}\left(\frac{ad}{zp_4}\right) \qquad (2)$$

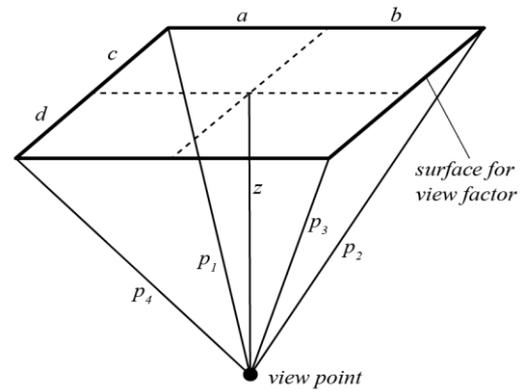Where Ω is the solid angle in steradians and all other variables refer to lengths in Figure 1:

Figure 1: Illustration for the calculation of solid angle.

To convert steradians to view factor, one simply divides Ω by the 4π steradians that exist over the sphere. While this method of calculation is fast, it is not generalizable to geometry that is non-orthogonal. As such, it is used in the simple web tool of Part 1 (Menchaca-Brandan et al., 2017) but it is not suitable for the complex geometry discussed in this paper.

One means of calculating view factors for more complex geometric cases involves ray-tracing, which projects a series of vectors in an evenly-spaced spherical pattern from a given point and counts the intersections of the rays with the surrounding surfaces (Figure 2).

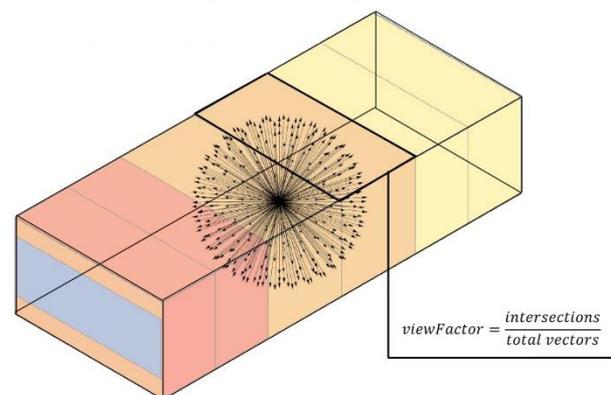$$viewFactor = \frac{intersections}{total\ vectors}$$

Figure 2: Ray tracing method for view factors.

While this method of obtaining view factors is more computationally intensive than solid angle calculations, it can be used for essentially any geometry. The specific method of ray tracing utilized in this paper generates vectors by means of the Tregenza sky dome, which is a division of the hemisphere originally devised for daylight calculations and produces a relatively even distribution of vectors (Tregneza and Wilson, 2013).

The tool presented in this paper computes the intersections of vectors with surfaces using the 3D geometry engine of the Rhino computer-aided design (CAD) software on which it runs. Altogether, the view factor to a surface is computed using equation 3:

$$F = \frac{1}{A_0} \sum_{i=1}^{N} B_i A_i \qquad (3)$$

Where B is the True/False (1/0) value for whether the intersection was successful A is the area of the given

Tregenza patch, and A_0 is the total area of the sphere. The individual vector intersections are summed over the whole sphere to determine the view factor to a given surface. Finally, these view factors are fed into Equation 1 and the PMV model to produce spatially resolved maps of the percentage of people dissatisfied (PPD) over the floor plan (Figure 3).
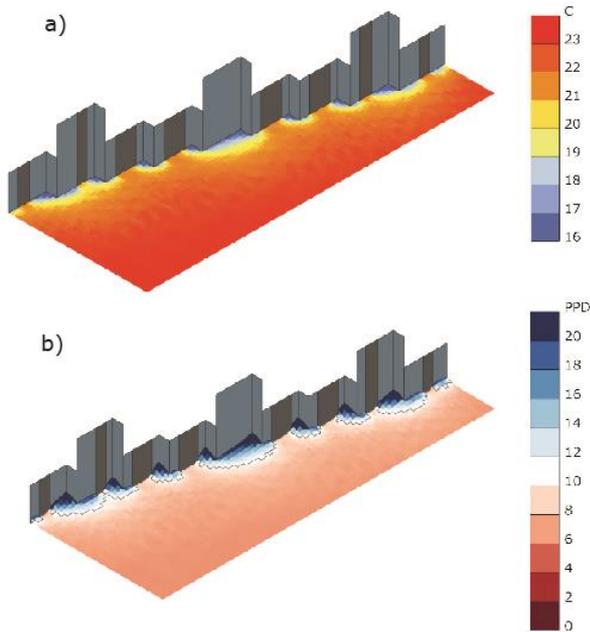

Figure 3: Map of MRT (a) and Percentage of People Dissatisfied (b) (PPD$_{Rad}$) for a complex geometric case.

It should also be noted that this same view factor calculation can be adapted to compute radiant asymmetry between the cold window and the warm interior. The critical difference is the multiplication of each intersection event by an angle factor, which essentially projects the hemispherical patch into a plane of radiant asymmetry. This factor can be computed using equation 4 below and, after the output is combined with equation 5, it can ultimately produce a map of radiant asymmetry discomfort (Figure 4).

$$F_{ang} = \cos(\emptyset) \qquad (4)$$

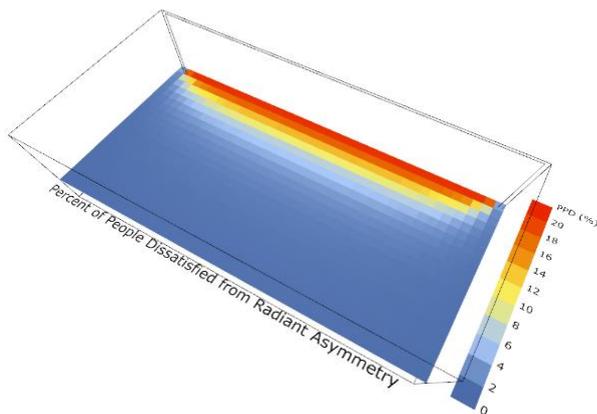$$PPD_{asym} = \frac{100}{1 + e^{(6.61 - 0.345 \times \Delta T)}} \qquad (5)$$

Figure 4: Map of Radiant Asymmetry Discomfort.

In these equations, F_{ang} is the angle factor, $\emptyset$ is the angle between the given vector and the plane of asymmetry, PPD_{asym} is the percentage of people dissatisfied from cold window radiant asymmetry, and ΔT is the radiant temperature difference from one side of a plane to the other (CEN, 2007). Although these formulas enable the inclusion of radiant asymmetry discomfort into the tool, several tests showed that radiant asymmetry from cold windows rarely exceeds the thresholds of ASHRAE or CEN, except in cases of large single pane windows (ASHRAE, 2010; CEN, 2007). Furthermore, for the cases tested in this study, such window-based radiant asymmetry discomfort only exceeded the thermal discomfort from full-body MRT and downdraft in cases where the interior thermostat set point was in excess of 27 C. Since these conditions are far from typical wintertime interior conditions of contemporary buildings, radiant asymmetry discomfort was excluded from the tool to decrease calculation times.

Downdraft with Varied Window Heights and Non-Rectangular Geometries

In addition to the method for spatially resolved MRT and radiant discomfort, a model that handles complex cases of window downdraft is also necessary to assess the need for perimeter heat. Heiselberg (1995) originally developed a simple parameterization of window downdraft speed that was later refined with further observations (Rueegg et al., 2001) and validated several CFD simulations (Manz and Frank, 2003):

$$v_{ankle} = \begin{cases} 0.083 \sqrt{H \Delta\theta} \ [m/s], & x < 0.4m \\ \frac{0.143}{x+1.32} \sqrt{H \Delta\theta} \ [m/s], & 0.4m \leq x \leq 2m \\ 0.043 \sqrt{H \Delta\theta} \ [m/s], & x > 2m \end{cases} \qquad (6)$$

$$\theta = T_{in} - T_{glass} \ [C]$$

Equation 6 indicates that the speed of the downdraft (v_{ankle}) is a function of the distance from the glass (x), the temperature difference between the indoor air and glass (θ) as well as the head height of the cold window (H). While this parameterization was originally developed using rectangular windows that have a consistent height, the formulas of the model suggest that the speed directly in front of the window is a function of the height of the window within the plane of airflow. As such, the generalization of this method to handle cases of varied window geometry simply requires an intersection of the window with the plane of airflow. By generating this plane of airflow using the shortest distance from a given point to the window, one can obtain custom values of H for equation 6, which can be used to make a corresponding 2D map of air velocity (Figure 5).
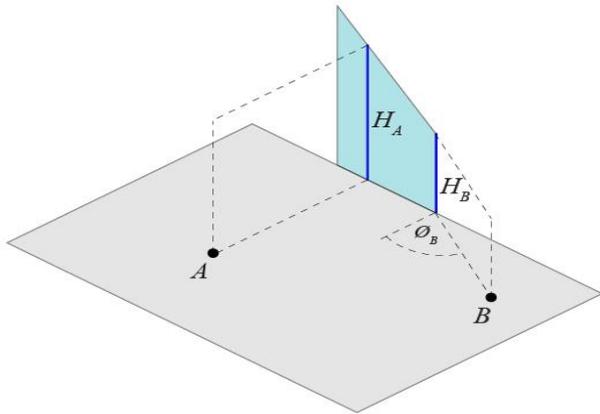
Figure 5: Intersection of airflow planes with a non-rectangular window geometry for a point in front of the window (A) and a point to the side (B).

Downdraft Spread over the Floor

In order to provide a spatial map of downdraft discomfort over the floor of a room, it is necessary to account for the spread of the downdraft plume. The original parameterization for the window downdraft (Equation 6) only describes the 1-dimensional condition of air speed immediately in front of the window and does not give guidance on 2D modelling the air speed over the entire floor. However, it is possible to derive an estimate of this spreading behaviour by noting three key characteristics of this airflow:

1) The spreading effect on the sides of the window should follow a similar pattern to the air immediately in front of the glass, with air speed gradually declining up until 2 meters from the window where it becomes fully entrained.

2) The cold downdraft should spread in all directions but should likely decrease in intensity as the angle between the window surface normal and the direction of flow increases. In this way, the forward momentum of the flow creates higher velocities in front of the window than on the sides.

3) Conservation of mass dictates that the total airflow immediately in front of the window should be equal to the total airflow at a certain distance away from the window.

Assuming that the height of the boundary layer does not change substantially in the first 2 meters from its source at the bottom of the glass, we can derive an equation that satisfies these three criteria. Specifically, one can write this equation in the following format:

$$v_{ankle} = f\left(g(x, H, \Delta\theta) \times \left(\frac{D}{1/S} + (1-S)\right)\right) \quad (7)$$

Where $g(x, H, \Delta\theta)$ is equation 6 (including the distance x to the widow and window height H in the plane of airflow), D is a directional factor that gradually ramps down the intensity of the air speed as the angle to the window plane decreases, and S is a spreading factor that ensures conservation of mass flow between the base of the

window and 2 meters away from the window. Assuming a linear relationship in how the air speed decreases in front of the glass to the sides, the variable D can be expressed as the following:

$$D = (90 - |\emptyset|)/90 \quad (8)$$

Where $\emptyset$ is the angle between the plane of airflow and the glass surface normal in degrees. For the variable S, a trial-and-error algorithm was run to match the mass flow immediately in front of the window at its source with the mass flow across a boundary 2 meters away from window. An S of 1 indicates a perfectly linear decrease of speed with angle all of the way to a speed of 0 at 90 degrees. An S that is less than 1 would only decrease the airflow to a certain speed. Ultimately, the guess-and-check algorithm found that an S of 0.97 ensured conservation of mass flow and the results of the model with this value were validated against a CFD study presented later in this paper. Taken together, the equation produces a spread of air velocity across the floor that can be plugged into the comfort model for PPD_{Draft} (Figure 6).
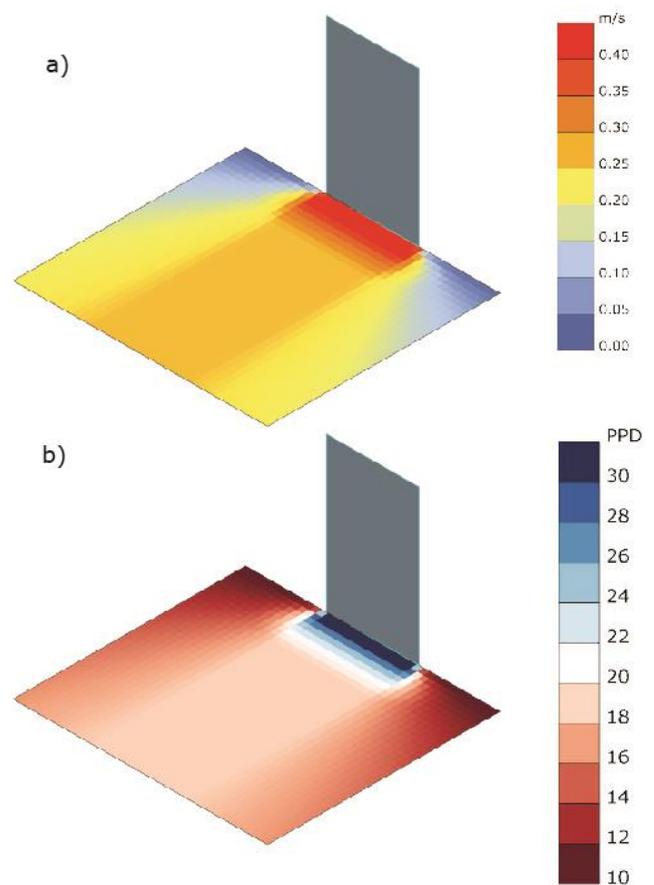

Figure 6: Distribution of downdraft speed over the floor (a) and corresponding PPD_{Draft} (b).

In order to deal with cases of multiple windows, the tool simply uses equation 7 and selects the largest of the air speeds amongst the windows that can cause downdraft. As such, it does not model the interaction of several downdraft plumes. However, as the window surfaces become closer together, the accuracy of this model should increase and future verifications with CFD may increase the accuracy of these situations.

Temporal Methods

Varied Climate Conditions and Occupancy

Up to this point, all modelled cases have assumed a steady state point-in-time analysis but this can be problematic, as buildings exist within dynamic and constantly changing conditions. At the least, one requires a standardized method for selecting the outdoor conditions for the thermal comfort analysis from the whole heating season and operating time of the building. The selection of a "design day" condition is a common practice used in the sizing of HVAC systems and could similarly be adapted to the selection of conditions to evaluate thermal discomfort here (ASHRAE, 2016). Borrowing from this methodology, it is often not practical to size an HVAC system using the worst possible hour of the year but rather the worst 1% case or 0.4% case over the entire distribution of climate conditions. Accordingly, the recommended method here for selecting outdoor conditions is to filter the outdoor temperatures to include only those within the occupied hours and take a temperature from the worst 1-0.4 percentile of these hours. This method has been built into the tool presented later in this paper.

Non-Steady State Building Physics

While the method above addresses the variation of outdoor climate and occupancy over the entire cold season, it does not address the effects of transient building physics on an hour-to-hour basis. As such, one still cannot account for the effects of thermal mass, warmer ceiling temperatures from air stratification, and many other phenomena that induce variations in surface temperature over the interior of a building. In order to address this, an alternate version of the tool presented in this paper has been developed that enables one to plug in surface temperatures from a building energy model to account for these transient phenomena (Sadeghipour and Pak, 2013). Using the same design day methods described in the previous section, Figure 7 displays a comparison of the steady state version of the tool with the transient version using office occupancy schedules and an air-based HVAC system. The thermal mass of a transient simulation results in slightly colder indoor temperatures for the early morning, when the design conditions occur. As the Figure illustrates, this can be enough to widen the discomfort region and push large fractions of the room above the threshold. However, the average error of this case is 1.2 PPD for radiant discomfort and 2.9 PPD for downdraft discomfort, which does not greatly alter the findings of the steady state tool.
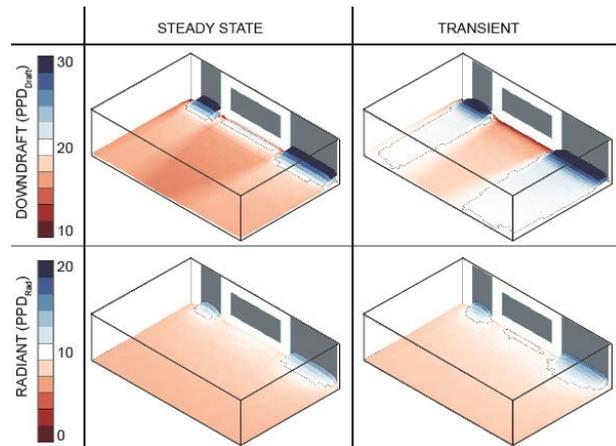
Figure 7: Comparison of PPD for the steady state and the transient tools.

The ability to plug in energy model results also enables one to test the impact of different heating delivery methods on the discomfort. Figure 8 displays the difference in discomfort that occurs between an air-based Fan Coil Unit system (interacting directly with the zone's air node) and a thermally massive radiant slab system.
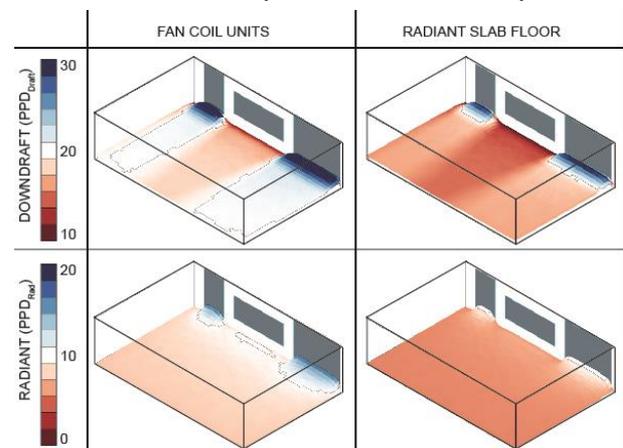
Figure 8: Comparison of air-based fan coil unit and radiant slab HVAC systems.

Validation of Methods

Since the tool presented in this paper is among the first of its kind to integrate both the full-body radiant and local downdraft discomfort calculations, there is no single other competing tool against in which the results can be validated (apart from the tool presented in Part 1 of this paper). However, each of the components of the calculation can be validated against competing methods or appropriate references can be listed for existing validations.

Validation of MRT Calculation

The steady-state calculation used to derive surface temperatures in the tool has been validated many times so much so that it has become a part of generally accepted building physics fundamentals (ASHRAE, 2013). Similarly, the transient calculations of surface temperature from EnergyPlus have also been validated

many times (Witte et al., 2004). The PMV model that estimates occupant dissatisfaction from MRT has been validated through hundreds of thermal comfort surveys of people in climate chambers (Fanger, 1973).

The only MRT-related method presented in this paper that has not undergone previous scientific validation is the ray tracing method that is used to compute view factors, which is different from that used by other ray-tracing engines like Radiance (Ward, 1994). Accordingly, Table 1 below compares the results of the tool's ray-traced view factors with that of the solid angle calculation described under the *Spatial Methods* section of this paper. It also presents the effect that this view factor difference has on the resulting MRT and PPD.

As the table indicates, the difference in view factors does not exceed 1%, which translates to an MRT difference that is less than 0.1°C and a final PPD that is not less than 0.1%. Accordingly, this ray tracing method is sufficiently accurate for the stated application of the tool.

	Distance From Façade (m)			
	1	**2**	**3**	**4**
Solid Angle View Fac	8.51%	5.92%	3.97%	2.73%
Ray-Traced View Fac	8.60%	5.87%	4.52%	2.41%
View Factor Error	0.09%	-0.05%	0.55%	-0.32%
Solid Angle MRT (°C)	21.29	21.61	21.82	21.94
Ray-Traced MRT (°C)	21.26	21.60	21.77	21.95
MRT Error (°C)	-0.03	-0.01	-0.05	0.01
Solid Angle PPD_{RAD}	6.98	6.57	6.33	6.19
Ray-Traced PPD_{RAD}	7.01	6.58	6.39	6.18
PPD_{RAD} Error	0.03	0.01	0.06	-0.01

Table 1: Comparison of the tool's ray tracing results against accurate solid angle view factors for a typical punched window case.

Validation of Downdraft Calculation

As previously noted, the steady-state calculation for 1-dimensional draft speed in front of the window has been validated and refined several times using both physical measurements (Heiselberg, 1995; Rueegg et al., 2001) and CFD simulations (Manz and Frank, 2003). In addition, the tool's model for calculating the percentage of people dissatisfied from ankle draft discomfort (PPD_{Draft}) has been validated against detailed climate chamber studies with over 100 subjects (Liu et al., 2016).

The only downdraft-related method presented in this paper that has not undergone a formal validation process is the calculation accounting for downdraft spread over the floor. Accordingly, Figure 9 compares the results from the tool's downdraft spreading model with that of a CFD study of the same geometry and temperature. The CFD study was run using the OpenFOAM engine and a mesh

grid size of 25 mm. It was allowed to run until steady state conditions were observed.
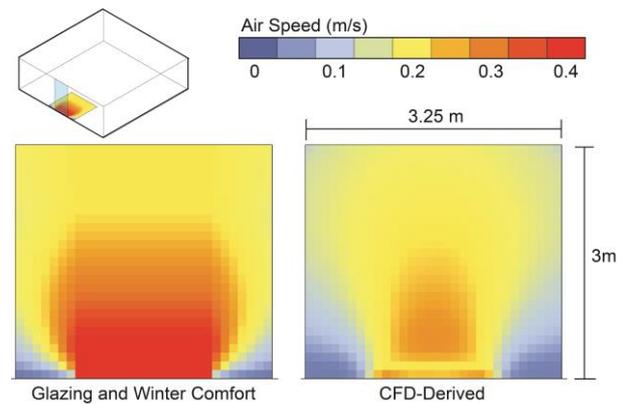

Figure 9: Comparison of the downdraft spread between CFD and the Glazing and Winter Comfort Tool.

As the figure indicates, the overall air speeds of the simple draft model are greater than that observed in the CFD and this finding is corroborated by the previous CFD validations of the 1-dimensional draft model (Manz and Frank, 2003). More specifically, the version of the 1-D model that is within the tool was purposely tweaked by Manz and Frank (2003) such that it is slightly conservative for most situations. In this way, it accounts for discrepancies between the model's idealized function and the varying flow rates received from the multiple CFD studies that Manz and Frank ran.

The conservative nature of this paper's proposed spreading model can be explained by the fact that it is derived from the conservative 1-D model and is simply an attempt to make this model obey conservation of mass flow. Accordingly, the spreading model proposed in this paper, while conservative, should be suitable for the stated application of ensuring occupants do not experience draft discomfort.

Interface

Inputs and the Visual Scripting Interface

Figure 10 illustrates how inputs are entered into the tool through the Grasshopper visual scripting interface. The implementation of the tool in Grasshopper means that the computer code for each calculation is wrapped into a discrete component with the inputs and outputs of the calculation exposed as variable names. For example, the component to calculate view factor takes into account the test points and glazing surfaces to output a list of view factors from the points to the surfaces. This view factor list can then be passed to a component that calculates MRT from them and so on. Figure 11 displays some of the new components that were developed for this tool and the fact that the calculation is broken down into these discrete components enables flexibility for advanced users. For example, the same components that are used to display the visual falsecolor output of PPD can also be used to display other types of data such as the air speed
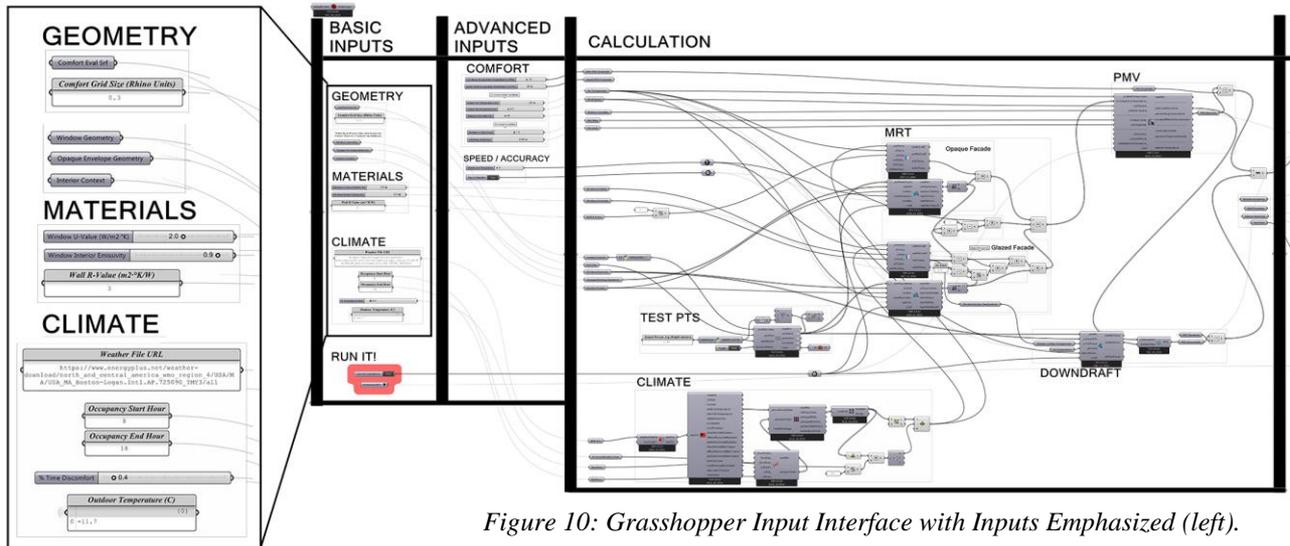
Figure 10: Grasshopper Input Interface with Inputs Emphasized (left).

distribution over the floor or MRT distirbution. Additionally, if someone has empirically-measured surface temperatures, they can plug this data into the relevant components to use them with the tool.

Outputs and 3D Visualization

As stated previously, the primary output of the tool is a falsecolor map of PPD with a boundary drawn around the region that does not satisfy the PPD threshold. However, it should be noted that the user has a choice of three possible faslecolor maps outlined in Figure 12. Two of these are the PPD_{Draft}, PPD_{Rad} previously described and the third is a combined visual of PPD that displays the relative percent difference from the respective PPD threshold. In this way, users can compare the relative effects of downdraft and radiant discomfort and visualize the full region of discomfort together.

Calculation Time and Parallelization

The most time-intensive portion of the tool is the view factor calculation, which accounts for slightly more than process in parallel has been included in the tool. The detailed façade condition of a double-height space in Figure 12 took 72 seconds to run on a standard quad-core machine. It should also be noted that the component-based workflow ensures that only the relevant components will be re-run when a given paramter is changed. For example, if the user changes the U-value, the time-intensive view factor calculation will not be re-run, thrreby enabling faster iteration with certain parameters.

Key Findings

Initial tests reveal that there can be significant deviation from the assumptions of the web tool in more complex geometric cases and when transient building physics are particularly relevant. Common spatial configurations like the corners of a building can have substantially more discomfort as a result of the interaction of the two glazed facades and an overall large view factor to glass. Interaction between double-height and single-height glazed spaces can result in unexpected regions of discomfort that are described by neither a purely single-height nor double-height case. The placement of furniture outside of the downdraft plume can be a viable means of mitigating discomfort, although its feasibility depends on both the height of the window and the acceptable offset distance of the furniture from the window edge. The use of a radiant floor slab system instead of an air-based heating system results in noticeable reductions of discomfort near the façade. While the general findings of Part 1 are corroborated here and the difference between the transient and steady state tools is not enough to undermine the web tool's conclusions, the nuances of these situations suggest that practitioners should test their more complex cases with the tool presented in this paper before proceeding with construction.

Limitations and Conclusions

In addition to the limitations of the method noted in Part 1 of this work (Menchaca-Brandan et al., 2017), the methods outlined here have a few additional restrictions.
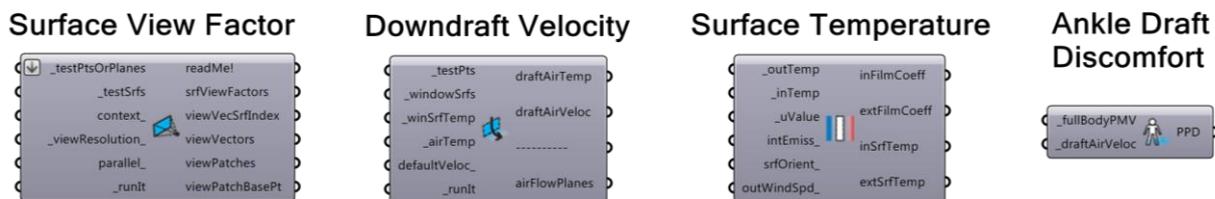

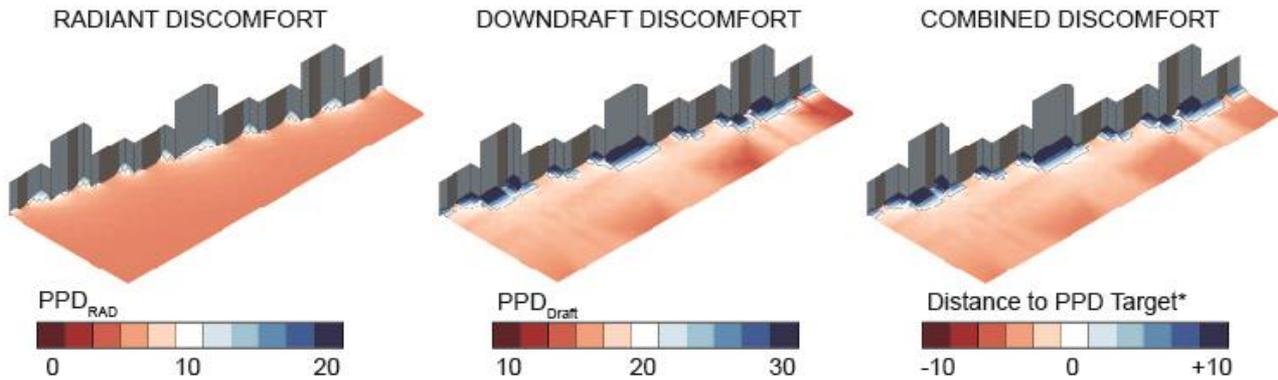*Figure 11: Custom components that were developed for the Glazing and Winter Comfort Tool.*

Figure 12: The three primary visual Outputs of the Tool.
*Here, the PPD Target is set at 10 for PPD_{RAD} and 20 for PPD_{Draft}, as per the recommendations of ASHRAE-55.
Negative values for the "Distance to PPD Target" are below both thresholds (acceptable).

Notably, the interactions between downdraft plumes are currently not accounted for and this will likely require future validations with CFD studies to model correctly. However, the tool's current methods of simply taking the greater of the two draft plume speeds is likely not too far from reality, where the increase in velocity from combining the two flows will be offset by the fact that colliding plumes cancel out the opposing components of their velocities. Accordingly, a small amount of caution should be taken with the results in between two downdraft plumes.

Another notable limitation is that the downdraft model used in the tool is based only on the cold interior temperature of the window and does not incorporate additional cold infiltration that could occur through cracks in the facade. As such, this tool should be used with caution in cases where the facade does not include typical contemporary strategies to mitigate infiltration (i.e., air + vapour barriers and caulked joints)

Ultimately, the tool presented here enables a more accurate check of strategies developed with the web tool of Part 1. Consequently, this helps avoid the need for additional safety factors in glazing selection or time-intensive CFD calculations to validate specific cases. Additionally, by accommodating a much wider range of design cases and incorporating flexibility into the input interface, this tool engenders creative approaches to addressing wintertime discomfort beyond the selection of window geometry and U-Value. For example, the tool presented here can evaluate creative solutions such as the positioning of seating away from the downdraft plume, interior surfaces that can block the radiant view to cold window surfaces, locally-heated surfaces, and even obstacles to downdraft. While the modelling procedure for downdraft obstacles is not outlined in this paper, studies have quantified the effects of common types of obstacles such as window sills and mullions (Heiselberg et al., 1996). Advanced users can account for their effects through the flexible visual scripting interface. Ultimately, this flexibility and increased accuracy enables early design goals of removing perimeter heat to sustain into later stages of development and, ultimately, into real buildings.

Acknowledgement

References

ASHRAE (2016) Standard 90.1: Energy Standard for Buildings Except Low-Rise Residential Buildings.

ASHRAE (2013) ASHRAE Handbook: Fundamentals.

ASHRAE (2010) Standard 55-2010: Thermal Environmental Conditions for Human Occupancy.

CEN, E. N. (2007). 15251-2007, Criteria for the Indoor Environment Including Thermal, Indoor Air Quality, Light and Noise. *Brussels: European Committee for Standardization*.

Chrenko, F. (1953). *Journal of the Institution of Heating &Ventilating Engineers*, 20, 375 and 21, 145.

Fanger, P. O. (1973). Assessment of Man's Thermal Comfort in Practice." *British Journal of Industrial Medicine* 30, no. 4: 313–324.

Heiselberg, P. (1994). Draught Risk From Cold Vertical Surfaces. *Building and Environment*, Vol 29, No. 3, 297-301.

Heiselberg, P.; Overby, H.; Bjørn, E. (1996). Energy-Efficient Measures to Avoid Downdraft from Large Glazed Facades. Aalborg: Dept. of Building Technology and Structural Engineering. *Indoor Environmental Technology*, Vol R9654, No. 62.

Hoyt, T; Arens, E.; Zhou, X.; Huang, L.; Zhang, H.;Schiavon, S. (2014), CBE MRT Tool. Center for the Built Environment, Uni. of California Berkeley, http://centerforthebuiltenvironment.github.io/mrt.

Liu, S.; Schiavon, S.; Kabanshi, A.; Nazaroff, W.. (2016). Predicted percentage of dissatisfied with ankle draft. Under review by *Indoor Air Journal*.

Manz, H. and Frank, T. (2003). Analysis of Thermal Comfort near Cold Vertical Surfaces by Means of Computational Fluid Dynamics. *Indoor Built Environment*. 13: 233-242.

Menchaca-Brandan, M A; Peterman, L; Baranova, V; Koltun, S. (2017). Glazing and Winter Comfort Part 1: An Accessible Web Tool for Early Design Decision-Making. *Proceedings of Building Simulation Conference 2017, San Francisco, CA*. Accepted Paper.

Newsham, G. (1992). Occupant movement and the thermal modelling of buildings. *Energy and Buildings*. Vol 18, No. 1, 57–64.

Rakha, T. (2015). Towards Comfortable and Walkable Cities: Spatially Resolved Outdoor Thermal Comfort Analysis Linked to Travel Survey-based Human Activity Schedules. *Chapter 2: Annual Thermal Comfort Metrics*.

Sadeghipour, M and Pak, M. (2013). Ladybug: a parametric environmental plugin for grasshopper to help designers create an environmentally-conscious design. *Proceedings of the 13th International IBPSA Conference*. Lyon, France Aug 25–30th.

Schellen, L.; Timmers, S.; Loomans, M.; Nelissen, E.; Hensen, J.; van Marken Lichtenbelt, W. (2012). Downdraught Assessment During Design: Experimental and Numerical Evaluation of a Rule of Thumb. *Building and Environment*, 57, 290–301.

Schiavon, S.; Rim, D.; Pasut, W.; Nazaroff, W. (2016). Sensation of draft at uncovered ankles for women exposed to displacement ventilation and underfloor air distribution systems. *Building and Environment*, 96, 228–236.

Svidt, K. and Heiselberg, P. (1995). CFD Calculations of the Air Flow Along a Cold Vertical Wall with an Obstacle. Aalborg: Dept. of Building Technology and Structural Engineering. *Indoor Environmental Technology*, Vol R9510, No. 49.

Toftum, J., Melikov, A; Tynel, A.; Bruzda, M; Fanger, P. (2003). Human Response to Air Movement—Evaluation of ASHRAE's Draft Criteria. *HVAC&R Research*, Vol 9, No. 2, 187-202.

Tregneza, P and Wilson, M. (2013). Daylighting: Architecture and Lighting Design. Routledge, 2 edition.

Ward, G. (1994). The Radiance Lighting Simulation and Rendering System. *Computer Graphics*, Orlando.

Webb, A. (2013). Mapping Comfort: An Analysis Method For Understanding Diversity in the Thermal Environment. *Proceedings of BS2013*, Chambery, France, pp. 1642–1648.

Witte, M; Henninger, R; Crawley, D (2004). Experience Testing Energyplus With The Ashrae 1052-RP Building Fabric Analytical Tests. *Proc. SimBuild*, Boulder, CO, USA